
3 Elastic-Plastic Fracture Mechanics

Linear elastic fracture mechanics (LEFM) is valid only as long as nonlinear material deformation is confined to a small region surrounding the crack tip. In many materials, it is virtually impossible to characterize the fracture behavior with LEFM, and an alternative fracture mechanics model is required.

Elastic-plastic fracture mechanics applies to materials that exhibit time-independent, nonlinear behavior (i.e., plastic deformation). Two elastic-plastic parameters are introduced in this chapter: the crack-tip-opening displacement (CTOD) and the J contour integral. Both parameters describe crack-tip conditions in elastic-plastic materials, and each can be used as a fracture criterion. Critical values of CTOD or J give nearly size-independent measures of fracture toughness, even for relatively large amounts of crack-tip plasticity. There are limits to the applicability of J and CTOD (Section 3.5 and Section 3.6), but these limits are much less restrictive than the validity requirements of LEFM.

3.1 CRACK-TIP-OPENING DISPLACEMENT

When Wells [1] attempted to measure K_c values in a number of structural steels, he found that these materials were too tough to be characterized by LEFM. This discovery brought both good news and bad news: High toughness is obviously desirable to designers and fabricators, but Wells' experiments indicated that the existing fracture mechanics theory was not applicable to an important class of materials. While examining fractured test specimens, Wells noticed that the crack faces had moved apart prior to fracture; plastic deformation had blunted an initially sharp crack, as illustrated in Figure 3.1. The degree of crack blunting increased in proportion to the toughness of the material. This observation led Wells to propose the opening at the crack tip as a measure of fracture toughness. Today, this parameter is known as CTOD.

In his original paper, Wells [1] performed an approximate analysis that related CTOD to the stress intensity factor in the limit of small-scale yielding. Consider a crack with a small plastic zone, as illustrated in Figure 3.2. Irwin [2] postulated that crack-tip plasticity makes the crack behave as if it were slightly longer (Section 2.8.1). Thus, we can estimate the CTOD by solving for the displacement at the physical crack tip, assuming an effective crack length of $a + r_y$. From Table 2.2, the displacement r_y behind the effective crack tip is given by

$$r_y = \frac{\kappa+1}{2\mu} K_I \sqrt{\frac{r_y}{2\pi}} = \frac{4}{E'} K_I \sqrt{\frac{r_y}{2\pi}} \quad (3.1)$$

where E' is the effective Young's modulus, as defined in Section 2.7. The Irwin plastic zone correction for plane stress is

$$r_y = \frac{1}{2\pi} \left(\frac{K_I}{\sigma_{YS}} \right)^2 \quad (3.2)$$

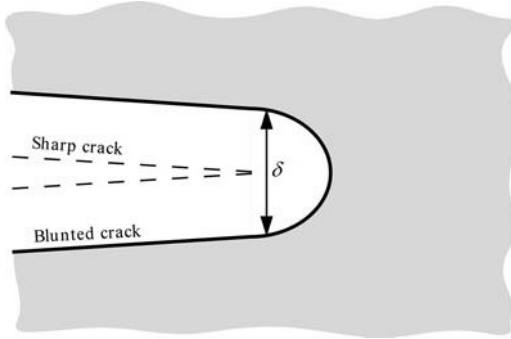


FIGURE 3.1 Crack-tip-opening displacement (CTOD). An initially sharp crack blunts with plastic deformation, resulting in a finite displacement (δ) at the crack tip.

Substituting Equation (3.2) into Equation (3.1) gives

$$\delta = 2u_y = \frac{4}{\pi} \frac{K_I^2}{\sigma_{YS} E} \quad (3.3)$$

where δ is the CTOD. Alternatively, CTOD can be related to the energy release rate by applying Equation (2.54):

$$\delta = \frac{4}{\pi} \frac{\mathcal{G}}{\sigma_{YS}} \quad (3.4)$$

Thus, in the limit of small-scale yielding, CTOD is related to \mathcal{G} and K_I . Wells postulated that CTOD is an appropriate crack-tip-characterizing parameter when LEFM is no longer valid. This assumption was shown to be correct several years later when a unique relationship between CTOD and the J integral was established (Section 3.3).

The strip-yield model provides an alternate means for analyzing CTOD [3]. Recall Section 2.8.2, where the plastic zone was modeled by yield magnitude closure stresses. The size of the strip-yield zone was defined by the requirement of finite stresses at the crack tip. The CTOD can be defined as the crack-opening displacement at the end of the strip-yield zone, as Figure 3.3 illustrates. According to this definition, CTOD in a through crack in an infinite plate subject to a remote tensile stress (Figure 2.3) is given by [3]

$$\delta = \frac{8\sigma_{YS}a}{\pi E} \ln \sec \left(\frac{\pi}{2} \frac{\sigma}{\sigma_{YS}} \right) \quad (3.5)$$

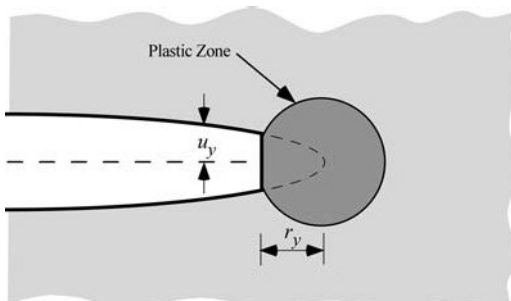


FIGURE 3.2 Estimation of CTOD from the displacement of the effective crack in the Irwin plastic zone correction.

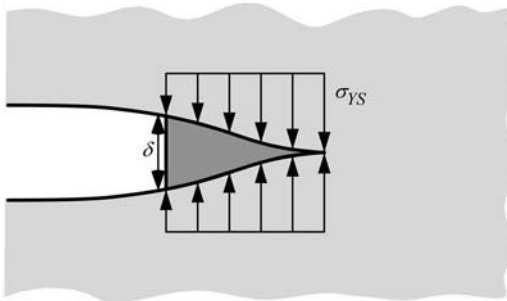


FIGURE 3.3 Estimation of CTOD from the strip-yield model. Taken from Burdekin, F.M. and Stone, D.E.W., “The Crack Opening Displacement Approach to Fracture Mechanics in Yielding Materials.” *Journal of Strain Analysis*, Vol. 1, 1966, pp. 145–153.

Equation (3.5) is derived in Appendix 3.1. Series expansion of the “ $\ln \sec$ ” term gives

$$\begin{aligned}\delta &= \frac{8\sigma_{YS}a}{\pi E} \left[\frac{1}{2} \left(\frac{\pi \sigma}{2 \sigma_{YS}} \right)^2 + \frac{1}{12} \left(\frac{\pi \sigma}{2 \sigma_{YS}} \right)^4 + \dots \right] \\ &= \frac{K_I^2}{\sigma_{YS} E} \left[1 + \frac{1}{6} \left(\frac{\pi \sigma}{2 \sigma_{YS}} \right)^2 + \dots \right]\end{aligned}\quad (3.6)$$

Therefore, as $\sigma/\sigma_{YS} \rightarrow 0$,

$$\delta = \frac{K_I^2}{\sigma_{YS} E} = \frac{G}{\sigma_{YS}} \quad (3.7)$$

which differs slightly from Equation (3.3).

The strip-yield model assumes plane stress conditions and a nonhardening material. The actual relationship between CTOD and K_I and G depends on stress state and strain hardening. The more general form of this relationship can be expressed as follows:

$$\delta = \frac{K_I^2}{m\sigma_{YS} E'} = \frac{G}{m\sigma_{YS}} \quad (3.8)$$

where m is a dimensionless constant that is approximately 1.0 for plane stress and 2.0 for plane strain.

There are a number of alternative definitions of CTOD. The two most common definitions, which are illustrated in Figure 3.4, are the displacement at the original crack tip and the 90° intercept. The latter definition was suggested by Rice [4] and is commonly used to infer CTOD in finite element measurements. Note that these two definitions are equivalent if the crack blunts in a semicircle.

Most laboratory measurements of CTOD have been made on edge-cracked specimens loaded in three-point bending (see Table 2.4). Early experiments used a flat paddle-shaped gage that was inserted into the crack; as the crack opened, the paddle gage rotated, and an electronic signal was sent to an x - y plotter. This method was inaccurate, however, because it was difficult to reach the crack tip with the paddle gage. Today, the displacement V at the crack mouth is measured, and the CTOD is inferred by assuming the specimen halves are rigid and rotate about a hinge point, as illustrated in Figure 3.5. Referring to this figure, we can estimate CTOD from a similar triangles construction:

$$\frac{\delta}{r(W-a)} = \frac{V}{r(W-a)+a}$$

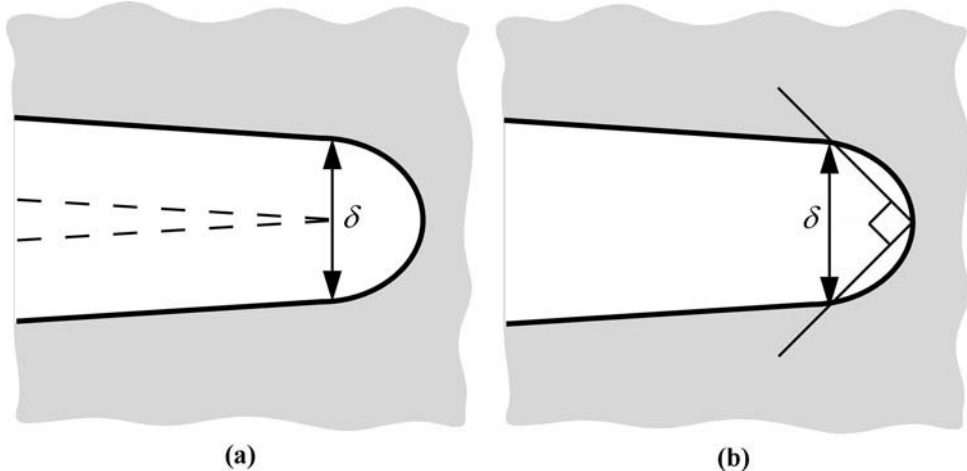


FIGURE 3.4 Alternative definitions of CTOD: (a) displacement at the original crack tip and (b) displacement at the intersection of a 90° vertex with the crack flanks.

Therefore

$$\delta = \frac{r(W-a)V}{r(W-a)+a} \quad (3.9)$$

where r is the rotational factor, a dimensionless constant between 0 and 1.

The hinge model is inaccurate when displacements are primarily elastic. Consequently, standard methods for CTOD testing [5, 6] typically adopt a modified hinge model, in which displacements are separated into elastic and plastic components; the hinge assumption is applied only to plastic displacements. Figure 3.6 illustrates a typical load (P) vs. displacement (V) curve from a CTOD test. The shape of the load-displacement curve is similar to a stress-strain curve: It is initially linear but deviates from linearity with plastic deformation. At a given point on the curve, the displacement is separated into elastic and plastic components by constructing a line parallel to the elastic loading line.

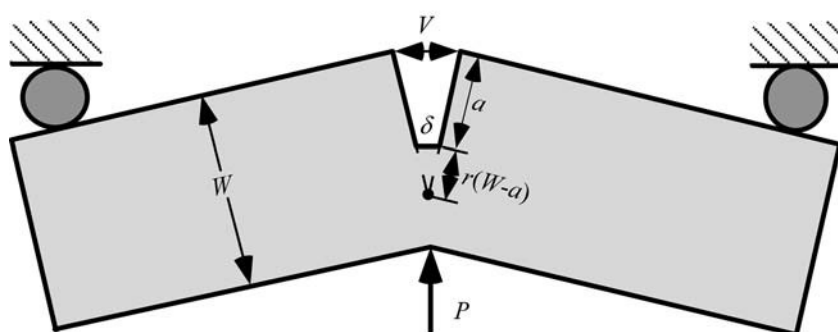


FIGURE 3.5 The hinge model for estimating CTOD from three-point bend specimens.

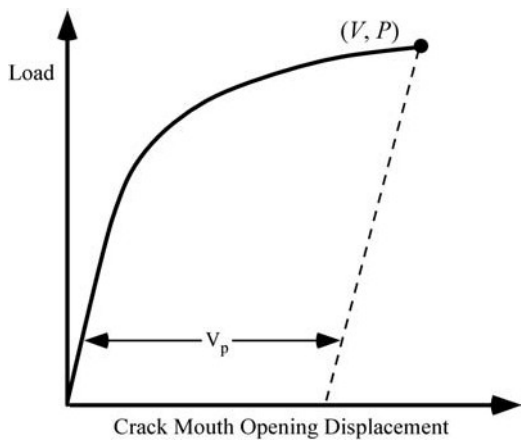


FIGURE 3.6 Determination of the plastic component of the crack-mouth-opening displacement.

The dashed line represents the path of unloading for this specimen, assuming the crack does not grow during the test. The CTOD in this specimen is estimated by

$$\delta = \delta_{el} + \delta_p = \frac{K_I^2}{m\sigma_{YS}E'} + \frac{r_p(W-a)V_p}{r_p(W-a)+a} \quad (3.10)$$

The subscripts *el* and *p* denote elastic and plastic components, respectively. The elastic stress intensity factor is computed by inserting the load and specimen dimensions into the appropriate expression in Table 2.4. The plastic rotational factor r_p is approximately 0.44 for typical materials and test specimens. Note that Equation (3.10) reduces to the small-scale yielding result (Equation (3.8)) for linear elastic conditions, but the hinge model dominates when $V \approx V_p$.

Further details of CTOD testing are given in Chapter 7. Chapter 9 outlines how CTOD is used in design.

3.2 THE *J* CONTOUR INTEGRAL

The *J* contour integral has enjoyed great success as a fracture characterizing parameter for nonlinear materials. By idealizing elastic-plastic deformation as nonlinear elastic, Rice [4] provided the basis for extending fracture mechanics methodology well beyond the validity limits of LEFM.

Figure 3.7 illustrates the uniaxial stress-strain behavior of elastic-plastic and nonlinear elastic materials. The loading behavior for the two materials is identical, but the material responses differ when each is unloaded. The elastic-plastic material follows a linear unloading path with the slope equal to Young's modulus, while the nonlinear elastic material unloads along the same path as it was loaded. There is a unique relationship between stress and strain in an elastic material, but a given strain in an elastic-plastic material can correspond to more than one stress value if the material is unloaded or cyclically loaded. Consequently, it is much easier to analyze an elastic material than a material that exhibits irreversible plasticity.

As long as the stresses in both materials in Figure 3.7 increase monotonically, the mechanical response of the two materials is identical. When the problem is generalized to three dimensions, it does not necessarily follow that the loading behavior of the nonlinear elastic and elastic-plastic materials is identical, but there are many instances where this is a good assumption (see Appendix 3.6). Thus an analysis that assumes nonlinear elastic behavior may be valid for an elastic-plastic material, provided no unloading occurs. The *deformation theory of plasticity*, which relates total strains to stresses in a material, is equivalent to nonlinear elasticity.

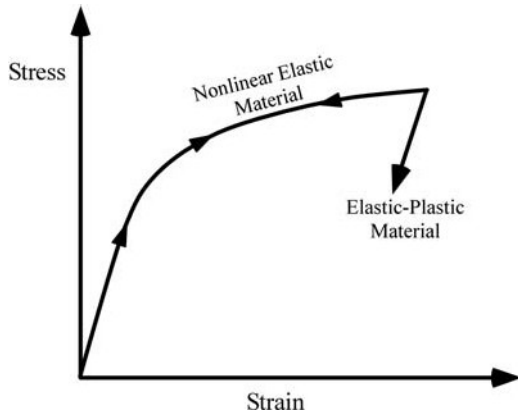


FIGURE 3.7 Schematic comparison of the stress-strain behavior of elastic-plastic and nonlinear elastic materials.

Rice [4] applied deformation plasticity (i.e., nonlinear elasticity) to the analysis of a crack in a nonlinear material. He showed that the nonlinear energy release rate J could be written as a path-independent line integral. Hutchinson [7] and Rice and Rosengren [8] also showed that J uniquely characterizes crack-tip stresses and strains in nonlinear materials. Thus the J integral can be viewed as both an energy parameter and a stress intensity parameter.

3.2.1 NONLINEAR ENERGY RELEASE RATE

Rice [4] presented a path-independent contour integral for the analysis of cracks. He then showed that the value of this integral, which he called J , is equal to the energy release rate in a nonlinear elastic body that contains a crack. In this section, however, the energy release rate interpretation is discussed first because it is closely related to concepts introduced in Chapter 2. The J contour integral is outlined in Section 3.2.2. Appendix 3.2 gives a mathematical proof, similar to what Rice [4] presented, that shows that this line integral is equivalent to the energy release rate in nonlinear elastic materials.

Equation (2.23) defines the energy release rate for linear materials. The same definition holds for nonlinear elastic materials, except that G is replaced by J :

$$J = -\frac{d\Pi}{dA} \quad (3.11)$$

where Π is the potential energy and A is the crack area. The potential energy is given by

$$\Pi = U - F \quad (3.12)$$

where U is the strain energy stored in the body and F is the work done by external forces. Consider a cracked plate which exhibits a nonlinear load-displacement curve, as illustrated in Figure 3.8. If the plate has unit thickness, $A = a$.¹ For load control

$$\Pi = U - P\Delta = -U^*$$

where U^* is the complimentary strain energy, defined as

$$U^* = \int_0^P \Delta dP \quad (3.13)$$

¹ It is important to remember that the energy release rate is defined in terms of the crack area, not crack length. Failure to recognize this can lead to errors and confusion when computing G or J for configurations other than edge cracks; examples include a through crack, where $dA = 2da$ (assuming unit thickness), and a penny-shaped crack, where $dA = 2\pi ad a$.

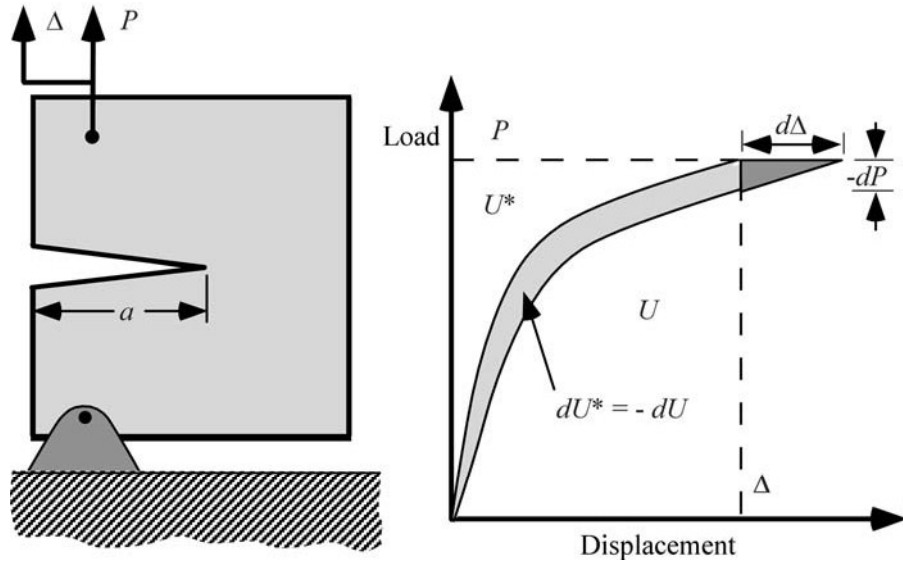


FIGURE 3.8 Nonlinear energy release rate.

Thus if the plate in Figure 3.8 is in load control, J is given by

$$J = \left(\frac{dU^*}{da} \right)_P \quad (3.14)$$

If the crack advances at a fixed displacement, $F = 0$, and J is given by

$$J = - \left(\frac{dU}{da} \right)_\Delta \quad (3.15)$$

According to Figure 3.8, dU^* for load control differs from $-dU$ for displacement control by the amount $\frac{1}{2} dP d\Delta$, which is vanishingly small compared to dU . Therefore, J for load control is equal to J for displacement control. Recall that we obtained this same result for \mathcal{Q} in Section 2.4.

By invoking the definitions for U and U^* , we can express J in terms of load and displacement:

$$\begin{aligned} J &= \left(\frac{\partial}{\partial a} \int_0^P \Delta dP \right)_P \\ &= \int_0^P \left(\frac{\partial \Delta}{\partial a} \right)_P dP \end{aligned} \quad (3.16)$$

or

$$\begin{aligned} J &= - \left(\frac{\partial}{\partial a} \int_0^\Delta P d\Delta \right)_\Delta \\ &= - \int_0^\Delta \left(\frac{\partial P}{\partial a} \right)_\Delta d\Delta \end{aligned} \quad (3.17)$$

Integrating Equation (3.17) by parts leads to a rigorous proof of what we have already inferred from Figure 3.8. That is, Equation (3.16) and Equation (3.17) are equal, and J is the same for fixed load and fixed grip conditions.

Thus, J is a more general version of the energy release rate. For the special case of a linear elastic material, $J = G$. Also

$$J = \frac{K_L^2}{E'} \quad (3.18)$$

for linear elastic Mode I loading. For mixed mode loading refer to Equation (2.63).

A word of caution is necessary when applying J to elastic-plastic materials. The energy release rate is normally defined as the potential energy that is *released* from a structure when the crack grows in an elastic material. However, much of the strain energy absorbed by an elastic-plastic material is not recovered when the crack grows or the specimen is unloaded; a growing crack in an elastic-plastic material leaves a plastic wake (Figure 2.6(b)). Thus the energy release rate concept has a somewhat different interpretation for elastic-plastic materials. Rather than defining the energy released from the body when the crack grows, Equation (3.15) relates J to the difference in energy absorbed by specimens with neighboring crack sizes. This distinction is important only when the crack grows (Section 3.4.2). See Appendix 4.2 and Chapter 12 for a further discussion of the energy release rate concept.

The energy release rate definition of J is useful for elastic-plastic materials when applied in an appropriate manner. For example, Section 3.2.5 describes how Equations (3.15)–(3.17) can be exploited to measure J experimentally.

3.2.2 J AS A PATH-INDEPENDENT LINE INTEGRAL

Consider an arbitrary counterclockwise path (Γ) around the tip of a crack, as in Figure 3.9. The J integral is given by

$$J = \int_{\Gamma} \left(w dy - T_i \frac{\partial u_i}{\partial x} ds \right) \quad (3.19)$$

where

w = strain energy density

T_i = components of the traction vector

u_i = displacement vector components

ds = length increment along the contour Γ

The strain energy density is defined as

$$w = \int_0^{e_{ij}} \sigma_{ij} d\varepsilon_{ij} \quad (3.20)$$

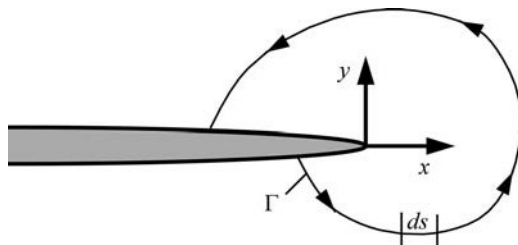


FIGURE 3.9 Arbitrary contour around the tip of a crack.

where σ_{ij} and ε_{ij} are the stress and strain tensors, respectively. The traction is a stress vector at a given point on the contour. That is, if we were to construct a free body diagram of the material inside of the contour, T_i would define the stresses acting at the boundaries. The components of the traction vector are given by

$$T_i = \sigma_{ij} n_j \quad (3.21)$$

where n_j are the components of the unit vector normal to Γ .

Rice [4] showed that the value of the J integral is independent of the path of integration around the crack. Thus J is called a *path-independent* integral. Appendix 3.2 demonstrates this path independence, and shows that Equation (3.19) is equal to the energy release rate.

3.2.3 J AS A STRESS INTENSITY PARAMETER

Hutchinson [7] and Rice and Rosengren [8] independently showed that J characterizes crack-tip conditions in a nonlinear elastic material. They each assumed a power law relationship between plastic strain and stress. If elastic strains are included, this relationship for uniaxial deformation is given by

$$\frac{\varepsilon}{\varepsilon_o} = \frac{\sigma}{\sigma_o} + \alpha \left(\frac{\sigma}{\sigma_o} \right)^n \quad (3.22)$$

where

σ_o = reference stress value that is usually equal to the yield strength

$\varepsilon_o = \sigma_o/E$

α = dimensionless constant

n = strain-hardening exponent.²

Equation (3.22) is known as the Ramberg-Osgood equation, and is widely used for curve-fitting stress-strain data. Hutchinson, Rice, and Rosengren showed that in order to remain path independent, stress-strain must vary as $1/r$ near the crack tip. At distances very close to the crack tip, well within the plastic zone, elastic strains are small in comparison to the total strain, and the stress-strain behavior reduces to a simple power law. These two conditions imply the following variation of stress and strain ahead of the crack tip:

$$\sigma_{ij} = k_1 \left(\frac{J}{r} \right)^{\frac{1}{n+1}} \quad (3.23a)$$

$$\varepsilon_{ij} = k_2 \left(\frac{J}{r} \right)^{\frac{n}{n+1}} \quad (3.23b)$$

where k_1 and k_2 are proportionality constants, which are defined more precisely below. For a linear elastic material, $n = 1$, and Equation (3.23) predicts a $1/\sqrt{r}$ singularity, which is consistent with LEFM theory.

² Although Equation (3.22) contains four material constants, there are only two fitting parameters. The choice of σ_o , which is arbitrary, defines ε_o ; a linear regression is then performed on a log-log plot of stress vs. plastic strain to determine α and n .

The actual stress and strain distributions are obtained by applying the appropriate boundary conditions (see Appendix 3.4):

$$\sigma_{ij} = \sigma_o \left(\frac{EJ}{\alpha \sigma_o^2 I_n r} \right)^{\frac{1}{n+1}} \tilde{\sigma}_{ij}(n, \theta) \quad (3.24a)$$

and

$$\epsilon_{ij} = \frac{\alpha \sigma_o}{E} \left(\frac{EJ}{\alpha \sigma_o^2 I_n r} \right)^{\frac{n}{n+1}} \tilde{\epsilon}_{ij}(n, \theta) \quad (3.24b)$$

where I_n is an integration constant that depends on n , and $\tilde{\sigma}_{ij}$ and $\tilde{\epsilon}_{ij}$ are the dimensionless functions of n and θ . These parameters also depend on the assumed stress state (i.e., plane stress or plane strain). Equation (3.24a) and Equation (3.24b) are called the HRR singularity, named after Hutchinson, Rice, and Rosengren [7, 8]. Figure 3.10 is a plot of I_n vs. n for plane stress and plane strain. Figure 3.11 shows the angular variation of $\tilde{\sigma}_{ij}(n, \theta)$ [7]. The stress components in Figure 3.11 are defined in terms of polar coordinates rather than x and y .

The J integral defines the amplitude of the HRR singularity, just as the stress intensity factor characterizes the amplitude of the linear elastic singularity. Thus J completely describes the conditions within the plastic zone. A structure in small-scale yielding has two singularity-dominated zones: one in the elastic region, where stress varies as $1/\sqrt{r}$, and one in the plastic zone where stress varies as $r^{-l/(n+1)}$. The latter often persists long after the linear elastic singularity zone has been destroyed by crack-tip plasticity.

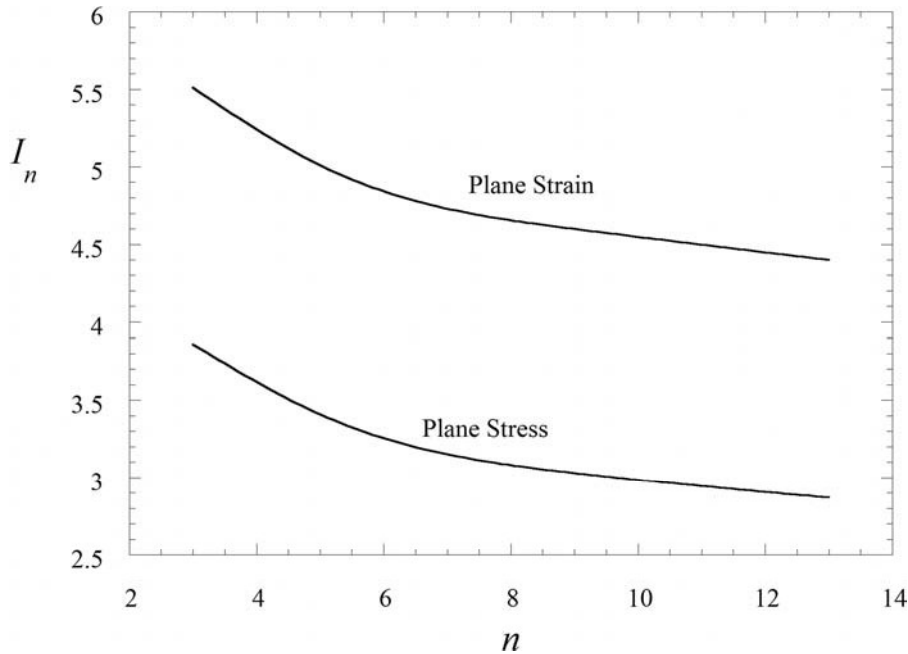


FIGURE 3.10 Effect of the strain-hardening exponent on the HRR integration constant.

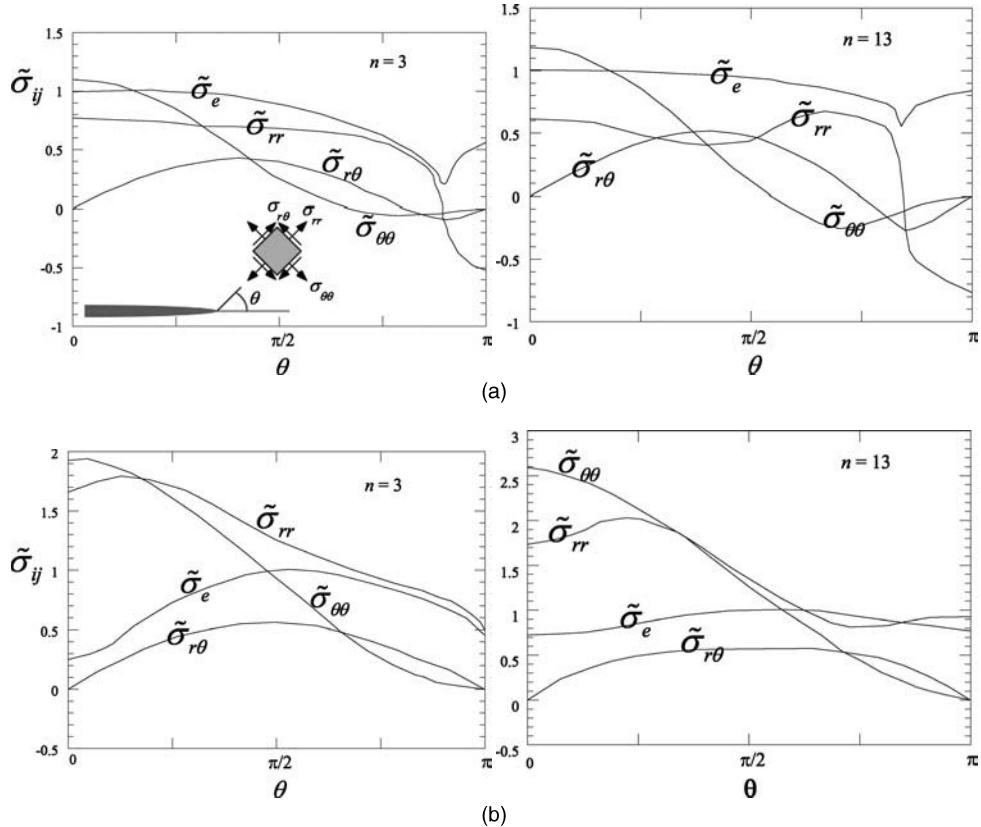


FIGURE 3.11 Angular variation of dimensionless stress for $n = 3$ and $n = 13$: (a) plane stress (b) plane strain. Taken from Hutchinson, J.W., "Singular Behavior at the End of a Tensile Crack Tip in a Hardening Material." *Journal of the Mechanics and Physics of Solids*, Vol. 16, 1968, pp. 13–31.

3.2.4 THE LARGE STRAIN ZONE

The HRR singularity contains the same apparent anomaly as the LEFM singularity; namely, both predict infinite stresses as $r \rightarrow 0$. However, the singular field does not persist all the way to the crack tip. The large strains at the crack tip cause the crack to blunt, which reduces the stress triaxiality locally. The blunted crack tip is a free surface; thus σ_{xx} must vanish at $r = 0$.

The analysis that leads to the HRR singularity does not consider the effect of the blunted crack tip on the stress fields, nor does it take account of the large strains that are present near the crack tip. This analysis is based on the small strain theory, which is the multi-axial equivalent of engineering strain in a tensile test. Small strain theory breaks down when strains are greater than ~ 0.10 (10%).

McMeeking and Parks [9] performed crack-tip finite element analyses that incorporated large strain theory and finite geometry changes. Some of their results are shown in Figure 3.12, which is a plot of stress normal to the crack plane vs. distance. The HRR singularity (Equation (3.24a)) is also shown on this plot. Note that both axes are nondimensionalized in such a way that both curves are invariant, as long as the plastic zone is small compared to the specimen dimensions.

The solid curve in Figure 3.12 reaches a peak when the ratio $x\sigma_0/J$ is approximately unity, and decreases as $x \rightarrow 0$. This distance corresponds approximately to twice the CTOD. The HRR singularity is invalid within this region, where the stresses are influenced by large strains and crack blunting.

The breakdown of the HRR solution at the crack tip leads to a similar question to one that was posed in Section 2.9: Is the J integral a useful fracture criterion when a blunting zone forms

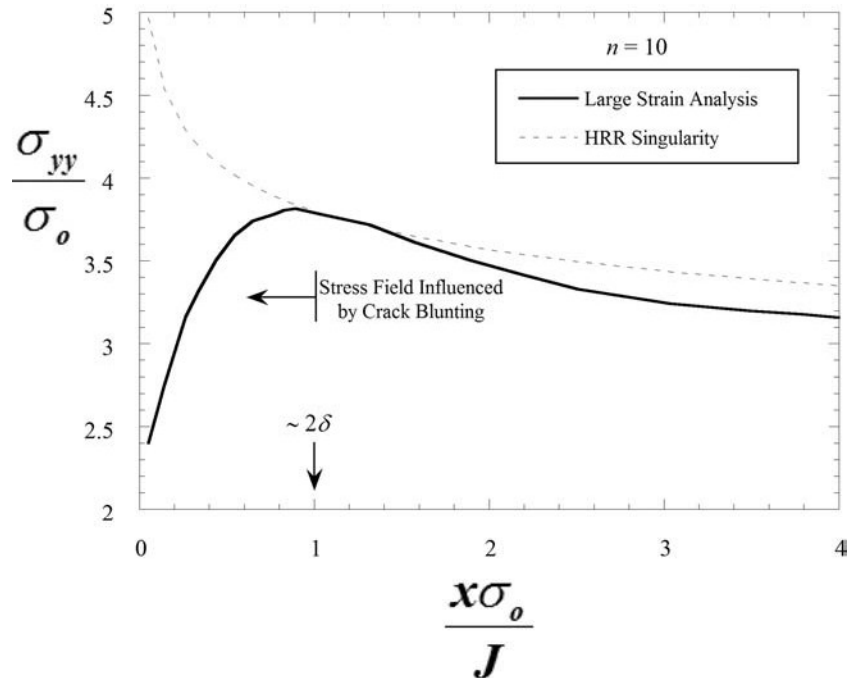


FIGURE 3.12 Large-strain crack-tip finite element results of McMeeking and Parks. Blunting causes the stresses to deviate from the HRR solution close to the crack tip. Taken from McMeeking, R.M. and Parks, D.M., “On Criteria for J -Dominance of Crack Tip Fields in Large-Scale Yielding.” *Elastic Plastic Fracture* ASTM STP 668, American Society for Testing and Materials, Philadelphia, PA, 1979, pp. 175–194.

at the crack tip? The answer is also similar to the argument offered in Section 2.9. That is, as long as there is a region *surrounding* the crack tip that can be described by Equation (3.24), the J integral uniquely characterizes crack-tip conditions, and a critical value of J is a size-independent measure of fracture toughness. The question of J controlled fracture is explored further in Section 3.5.

3.2.5 LABORATORY MEASUREMENT OF J

When the material behavior is linear elastic, the calculation of J in a test specimen or structure is relatively straightforward because $J = G$, and G is uniquely related to the stress intensity factor. The latter quantity can be computed from the load and crack size, assuming a K solution for that particular geometry is available.

Computing the J integral is somewhat more difficult when the material is nonlinear. The principle of superposition no longer applies, and J is not proportional to the applied load. Thus a simple relationship between J , load, and crack length is usually not available.

One option for determining J is to apply the line integral definition Equation (3.19) to the configuration of interest. Read [10] has measured the J integral in test panels by attaching an array of strain gages in a contour around the crack tip. Since J is path independent and the choice of contour is arbitrary, he selected a contour in such a way as to simplify the calculation of J as much as possible. This method can also be applied to finite element analysis, i.e., stresses, strains, and displacements can be determined along a contour and J can then be calculated according to Equation (3.19). However, the contour method for determining J is impractical in most cases. The instrumentation required for experimental measurements of the contour integral is highly cumbersome, and the contour method is also not very attractive in numerical analysis (see Chapter 12).

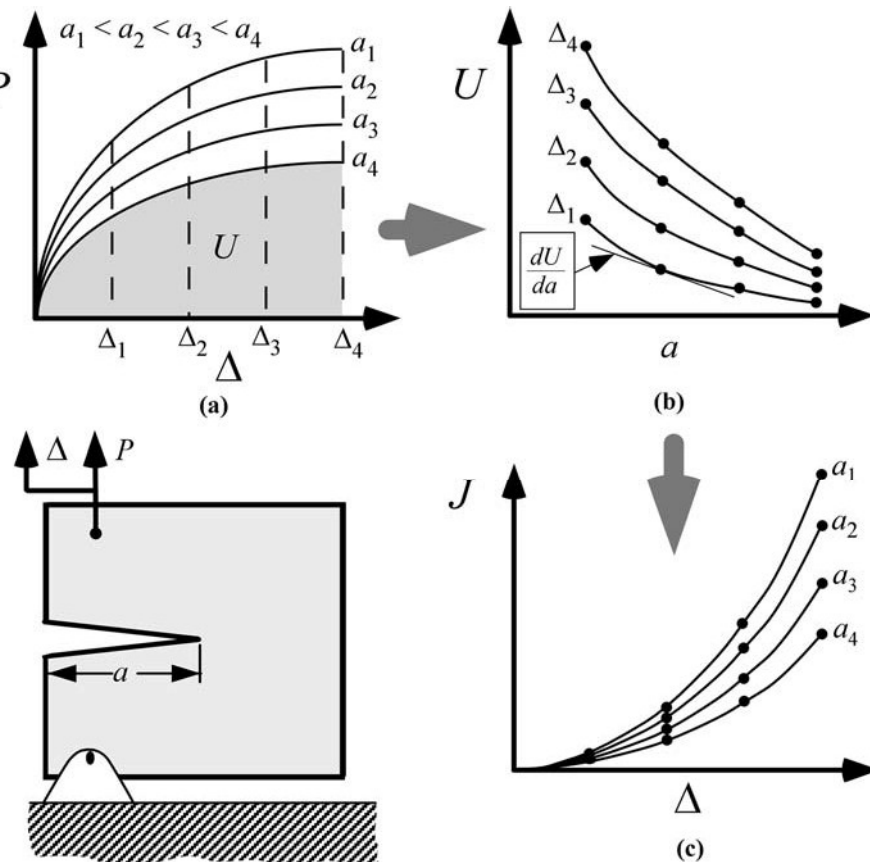


FIGURE 3.13 Schematic of early experimental measurements of J , performed by Landes and Begley. Taken from Begley, J.A. and Landes, J.D., “The J -Integral as a Fracture Criterion.” ASTM STP 514, American Society for Testing and Materials, Philadelphia, PA, 1972, pp. 1–20; Landes, J.D. and Begley, J.A., “The Effect of Specimen Geometry on J_c .” ASTM STP 514, American Society for Testing and Materials, Philadelphia, PA, 1972, pp. 24–29.

A much better method for determining J numerically is outlined in Chapter 12. More practical experimental approaches are developed below and are explored further in Chapter 7.

Landes and Begley [11, 12], who were among the first to measure J experimentally, invoked the energy release rate definition of J (Equation (3.11)). Figure 3.13 schematically illustrates their approach. They obtained a series of test specimens of the same size, geometry, and material and introduced cracks of various lengths.³ They deformed each specimen and plotted load vs. displacement (Figure 3.13(a)). The area under a given curve is equal to U , the energy absorbed by the specimen. Landes and Begley plotted U vs. crack length at various fixed displacements (Fig. 3.13(b)). For an edge-cracked specimen of thickness B , the J integral is given by

$$J = -\frac{1}{B} \left(\frac{\partial U}{\partial a} \right)_\Delta \quad (3.25)$$

Thus J can be computed by determining the slope of the tangent to the curves in Figure 3.13(b). Applying Equation (3.25) leads to Figure 3.13(c), a plot of J vs. displacement at various crack

³ See Chapter 7 for a description of fatigue-precracking procedures for test specimens.

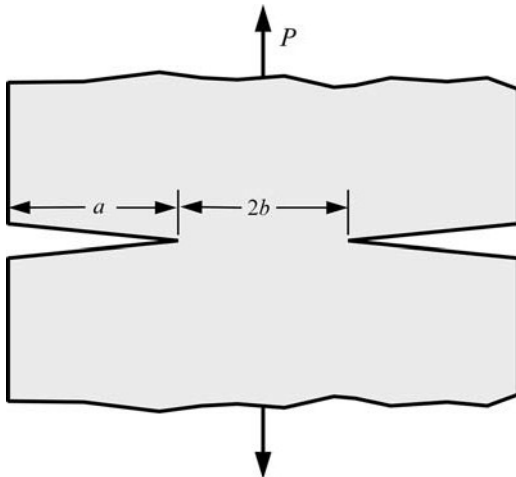


FIGURE 3.14 Double-edge-notched tension (DENT) panel.

lengths. The latter is a calibration curve, which only applies to the material, specimen size, specimen geometry, and temperature for which it was obtained. The Landes and Begley approach has obvious disadvantages, since multiple specimens must be tested and analyzed to determine J in a particular set of circumstances.

Rice et al. [13] showed that it was possible, in certain cases, to determine J directly from the load displacement curve of a single specimen. Their derivations of J relationships for several specimen configurations demonstrate the usefulness of dimensional analysis.⁴

Consider a double-edge-notched tension panel of unit thickness (Figure 3.14). Cracks of length a on opposite sides of the panel are separated by a ligament of length $2b$. For this configuration, $dA = 2da = -2db$ (see Footnote 1); Equation (3.16) must be modified accordingly:

$$J = \frac{1}{2} \int_0^P \left(\frac{\partial \Delta}{\partial a} \right)_P dP = -\frac{1}{2} \int_0^P \left(\frac{\partial \Delta}{\partial b} \right)_P dP \quad (3.26)$$

In order to compute J from the above expression, it is necessary to determine the relationship between load, displacement, and panel dimensions. Assuming an isotropic material that obeys a Ramberg-Osgood stress-strain law (Equation (3.22)), the dimensional analysis gives the following functional relationship for displacement:

$$\Delta = b\Phi\left(\frac{P}{\sigma_o b}; \frac{a}{b}; \frac{\sigma_o}{E}; v; \alpha; n\right) \quad (3.27)$$

where Φ is a dimensionless function. For fixed material properties, we need only consider the load and specimen dimensions. For reasons described below, we can simplify the functional relationship for displacement by separating Δ into elastic and plastic components:

$$\Delta = \Delta_{el} + \Delta_p \quad (3.28)$$

⁴ See Section 1.5 for a review of the fundamentals of dimensional analysis.

Substituting Equation (3.28) into Equation (3.26) leads to a relationship for the elastic and plastic components of J :

$$\begin{aligned} J &= -\frac{1}{2} \int_0^P \left[\left(\frac{\partial \Delta_{el}}{\partial b} \right)_p + \left(\frac{\partial \Delta_p}{\partial b} \right)_p \right] dP \\ &= \frac{K_I^2}{E'} - \frac{1}{2} \int_0^P \left(\frac{\partial \Delta_p}{\partial b} \right)_p dP \end{aligned} \quad (3.29)$$

where $E' = E$ for plane stress and $E' = E/(1 - \nu^2)$ for plane strain, as defined in Chapter 2. Thus we need only be concerned about plastic displacements because a solution for the elastic component of J is already available (Table 2.4). If plastic deformation is confined to the ligament between the crack tips (Figure 3.14(b)), we can assume that b is the only length dimension that influences Δ_p . That is a reasonable assumption, provided the panel is deeply notched so that the average stress in the ligament is substantially higher than the remote stress in the gross cross section. We can define a new function for Δ_p :

$$\Delta_p = bH\left(\frac{P}{b}\right) \quad (3.30)$$

Note that the net-section yielding assumption has eliminated the dependence on the a/b ratio. Taking a partial derivative with respect to the ligament length gives

$$\left(\frac{\partial \Delta_p}{\partial b} \right)_P = H\left(\frac{P}{b}\right) - H'\left(\frac{P}{b}\right)\frac{P}{b}$$

where H' denotes the first derivative of the function H . We can solve for H' by taking a partial derivative of Equation (3.30) with respect to load:

$$\left(\frac{\partial \Delta_p}{\partial P} \right)_b = H'\left(\frac{P}{b}\right)$$

Therefore

$$\left(\frac{\partial \Delta_p}{\partial b} \right)_P = \frac{1}{b} \left[\Delta_p - P \left(\frac{\partial \Delta_p}{\partial P} \right)_b \right] \quad (3.31)$$

Substituting Equation (3.31) into Equation (3.29) and integrating by parts gives

$$J = \frac{K_I^2}{E'} + \frac{1}{2b} \left[2 \int_0^{\Delta_p} P d\Delta_p - P \Delta_p \right] \quad (3.32)$$

Recall that we assumed a unit thickness at the beginning of this derivation. In general, the plastic term must be divided by the plate thickness; the term in square brackets, which depends on the load displacement curve, is normalized by the net cross-sectional area of the panel. The J integral has units of energy/area.

Another example from the Rice et al. article [13] is an edge-cracked plate in bending (Figure 3.15). In this case they chose to separate displacements along somewhat different lines from the previous problem. If the plate is subject to a bending moment M , it would displace by an angle Ω_{nc} if no crack were present, and an additional amount Ω_c when the plate is cracked.

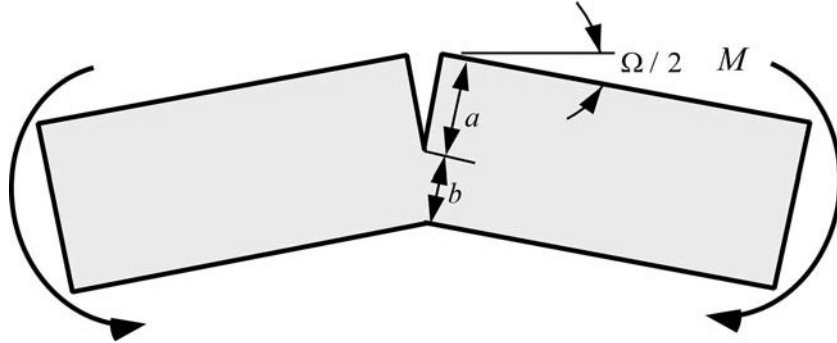


FIGURE 3.15 Edge-cracked plate in pure bending.

Thus the total angular displacement can be written as

$$\Omega = \Omega_{nc} + \Omega_c \quad (3.33)$$

If the crack is deep, $\Omega_c \gg \Omega_{nc}$. The energy absorbed by the plate is given by

$$U = \int_0^{\Omega} M d\Omega \quad (3.34)$$

When we differentiate U with respect to the crack area in order to determine J , only Ω_c contributes to the energy release rate because Ω_{nc} is not a function of crack size, by definition. By analogy with Equation (3.16), J for the cracked plate in bending can be written as

$$J = \int_0^M \left(\frac{\partial \Omega_c}{\partial a} \right)_M dM = - \int_0^M \left(\frac{\partial \Omega_c}{\partial b} \right)_M dM \quad (3.35)$$

If the material properties are fixed, dimensional analysis leads to

$$\Omega_c = F\left(\frac{M}{b^2}\right) \quad (3.36)$$

assuming the ligament length is the only relevant length dimension, which is reasonable if the crack is deep. When Equation (3.36) is differentiated with respect to b and inserted into Equation (3.35), the resulting expression for J is as follows:

$$J = \frac{2}{b} \int_0^{\Omega_c} M d\Omega_c \quad (3.37)$$

The decision to separate Ω into “crack” and “no-crack” components was somewhat arbitrary. The angular displacement could have been divided into elastic and plastic components as in the previous example. If the crack is relatively deep, Ω_{nc} should be entirely elastic, while Ω_c may contain both elastic and plastic contributions. Therefore, Equation (3.37) can be written as

$$J = \frac{2}{b} \left[\int_0^{\Omega_{c(el)}} M d\Omega_{c(el)} + \int_0^{\Omega_p} M d\Omega_p \right]$$

or

$$J = \frac{K_I^2}{E'} + \frac{2}{b} \int_0^{\Omega_p} M d\Omega_p \quad (3.38)$$

Conversely, the prior analysis on the double-edged cracked plate in tension could have been written in terms of Δ_c and Δ_{nc} . Recall, however, that the dimensional analysis was simplified in each case (Equation (3.30) and Equation (3.36)) by assuming a negligible dependence on a/b . This turns out to be a reasonable assumption for plastic displacements in deeply notched DENT panels, but less so for elastic displacements. Thus while elastic and plastic displacements due to the crack can be combined to compute J in bending (Equation (3.37)), it is not advisable to do so for tensile loading. The relative accuracy and the limitations of Equation (3.32) and Equation (3.37) are evaluated in Chapter 9.

In general, the J integral for a variety of configurations can be written in the following form:

$$J = \frac{\eta U_c}{Bb} \quad (3.39)$$

where η is a dimensionless constant. Note that Equation (3.39) contains the actual thickness, while the above derivations assumed a unit thickness for convenience. Equation (3.39) expresses J as the energy absorbed, divided by the cross-sectional area, times a dimensionless constant. For a deeply cracked plate in pure bending, $\eta = 2$. Equation (3.39) can be separated into elastic and plastic components:

$$\begin{aligned} J &= \frac{\eta_{el} U_{c(el)}}{Bb} + \frac{\eta_p U_p}{Bb} \\ &= \frac{K_I^2}{E'} + \frac{\eta_p U_p}{Bb} \end{aligned} \quad (3.40)$$

EXAMPLE 3.1

Determine the plastic η factor for the DENT configuration, assuming the load-plastic displacement curve follows a power law:

$$P = C \Delta_p^N$$

Solution: The plastic energy absorbed by the specimen is given by

$$U_p = \int_0^{\Delta_p} \Delta_p^N d\Delta_p = \frac{C \Delta_p^{N+1}}{N+1} = \frac{P \Delta p}{N+1}$$

Comparing Equation (3.32) and Equation (3.40) and solving for η_p gives

$$\eta_p = \frac{P \Delta p \left(\frac{2}{N+1} - 1 \right)}{\frac{P \Delta p}{N+1}} = 1 - N$$

For a nonhardening material, $N = 0$ and $\eta_p = 1$.

3.3 RELATIONSHIPS BETWEEN J AND CTOD

For linear elastic conditions, the relationship between CTOD and G is given by Equation (3.8). Since $J = G$ for linear elastic material behavior, these equations also describe the relationship between CTOD and J in the limit of small-scale yielding. That is

$$J = m\sigma_{ys}\delta \quad (3.41)$$

where m is a dimensionless constant that depends on the stress state and material properties. It can be shown that Equation (3.41) applies well beyond the validity limits of LEFM.

Consider, for example, a strip-yield zone ahead of a crack tip, as illustrated in Figure 3.16. Recall (from Chapter 2) that the strip-yield zone is modeled by surface tractions along the crack face. Let us define a contour Γ along the boundary of this zone. If the damage zone is long and slender, i.e., if $\rho \gg \delta$, the first term in the J contour integral (Equation 3.19) vanishes because $dy = 0$. Since the only surface tractions within ρ are in the y direction, $n_y = 1$ and $n_x = n_z = 0$. Thus the J integral is given by

$$J = \int_{\Gamma} \sigma_{yy} \frac{\partial u_y}{\partial x} ds \quad (3.42)$$

Let us define a new coordinate system with the origin at the tip of the strip-yield zone: $X = \rho - x$. For a fixed δ , σ_{yy} and u_y depend only on X , provided ρ is small compared to the in-plane dimensions of the cracked body. The J integral becomes

$$\begin{aligned} J &= 2 \int_0^{\rho} \sigma_{yy}(X) \left(\frac{du_y(X)}{dX} \right) dX \\ &= \int_0^{\delta} \sigma_{yy}(\delta) d\delta \end{aligned} \quad (3.43)$$

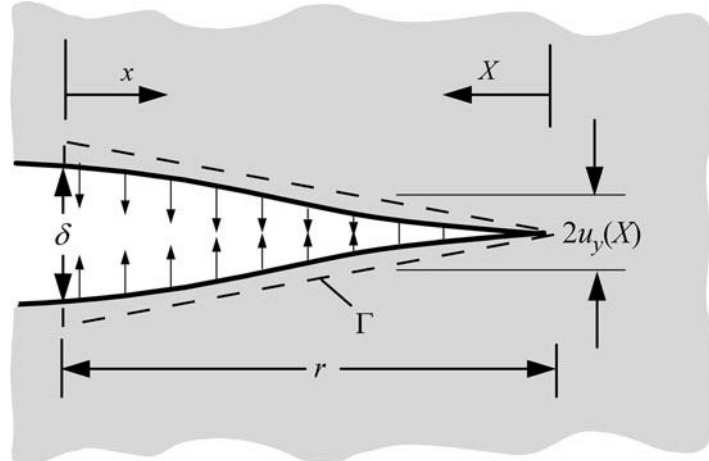


FIGURE 3.16 Contour along the boundary of the strip-yield zone ahead of a crack tip.

where $\delta = 2u_y (X = \rho)$. Since the strip-yield model assumes $\sigma_{yy} = \sigma_{ys}$ within the plastic zone, the J -CTOD relationship is given by

$$J = \sigma_{ys}\delta \quad (3.44)$$

Note the similarity between Equation (3.44) and Equation (3.7). The latter was derived from the strip-yield model by neglecting the higher-order terms in a series expansion; no such assumption was necessary to derive Equation (3.44). Thus the strip-yield model, which assumes plane stress conditions and a nonhardening material, predicts that $m = 1$ for both linear elastic and elastic-plastic conditions.

Shih [14] provided further evidence that a unique J -CTOD relationship applies well beyond the validity limits of LEFM. He evaluated the displacements at the crack tip implied by the HRR solution and related the displacement at the crack tip to J and flow properties. According to the HRR solution, the displacements near the crack tip are as follows:

$$u_i = \frac{\alpha\sigma_o}{E} \left(\frac{EJ}{\alpha\sigma_o^2 I_n r} \right)^{\frac{n}{n+1}} r \tilde{u}_i(\theta, n) \quad (3.45)$$

where \tilde{u}_i is a dimensionless function of θ and n , analogous to $\tilde{\sigma}_{ij}$ and $\tilde{\varepsilon}_{ij}$ (Equation (3.24)). Shih [14] invoked the 90° intercept definition of CTOD, as illustrated in Figure 3.4(b). This 90° intercept construction is examined further in Figure 3.17. The CTOD is obtained by evaluating u_x and u_y at $r = r^*$ and $\theta = \pi$:

$$\frac{\delta}{2} = u_y(r^*, \pi) = r^* - u_x(r^*, \pi) \quad (3.46)$$

Substituting Equation (3.46) into Equation (3.45) and solving for r^* gives

$$r^* = \left(\frac{\alpha\sigma_o}{E} \right)^{1/n} \left\{ \tilde{u}_x(\pi, n) + \tilde{u}_y(\pi, n) \right\}^{\frac{n+1}{n}} \frac{J}{\sigma_o I_n} \quad (3.47)$$

Setting $\delta = 2u_y(r^*, \pi)$ leads to

$$\delta = \frac{d_n J}{\sigma_o} \quad (3.48)$$

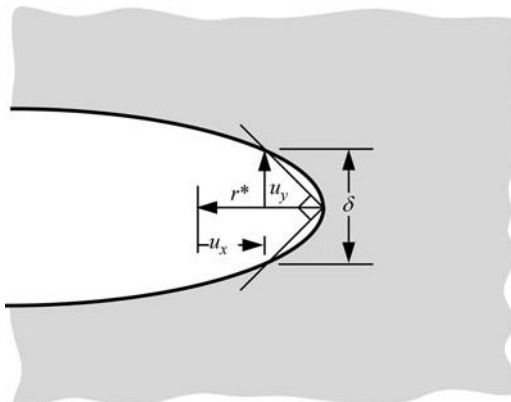


FIGURE 3.17 Estimation of CTOD from a 90° intercept construction and HRR displacements.

where d_n is a dimensionless constant, given by

$$d_n = \frac{2\tilde{u}_y(\pi, n) \left[\frac{\alpha\sigma_o}{E} \{ \tilde{u}_x(\pi, n) + \tilde{u}_y(\pi, n) \} \right]^{1/n}}{I_n} \quad (3.49)$$

Figure 3.18 shows plots of d_n for $\alpha=1.0$, which exhibits a strong dependence on the strain-hardening exponent and a mild dependence on $\alpha\sigma_o/E$. A comparison of Equation (3.41) and

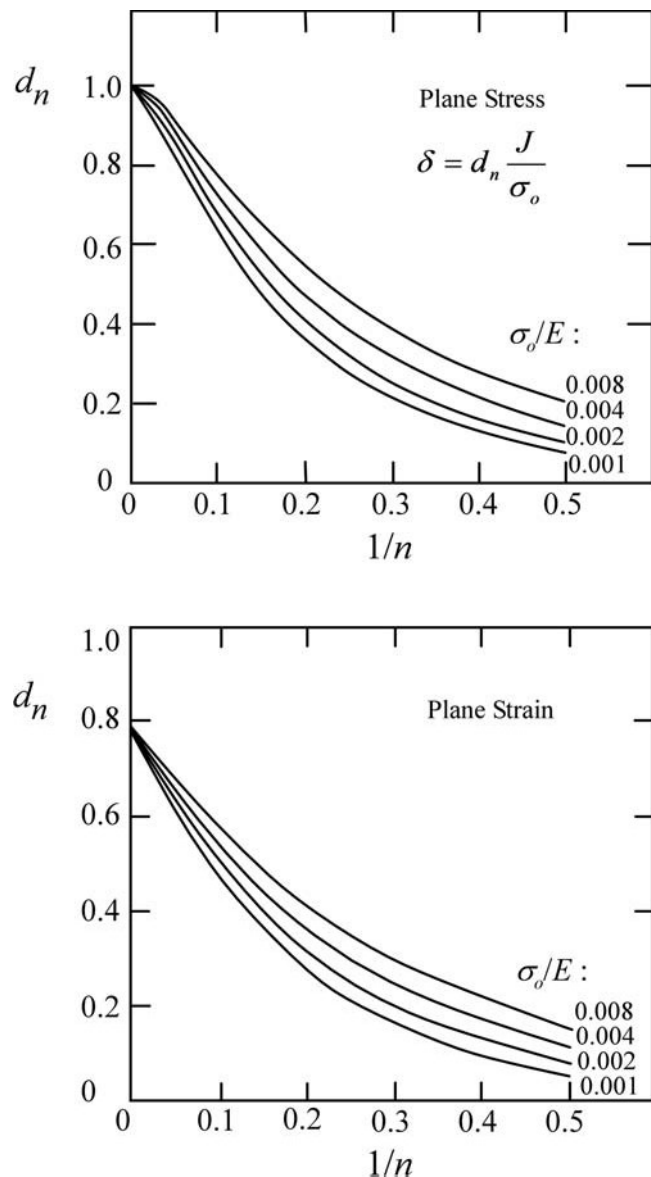


FIGURE 3.18 Predicted J -CTOD relationships for plane stress and plane strain, assuming $\alpha=1$. For $\alpha \neq 1$, the above values should be multiplied by $\alpha^{1/n}$. Taken from Shih, C.F. "Relationship between the J -Integral and the Crack Opening Displacement for Stationary and Extending Cracks." *Journal of the Mechanics and Physics of Solids*, Vol. 29, 1981, pp. 305–326.

Equation (3.48) indicates that $d_n = 1/m$, assuming $\sigma_o = \sigma_{YS}$ (see Footnote 2). According to Figure 3.18(a), $d_n = 1.0$ for a nonhardening material ($n = \infty$) in plane stress, which agrees with the strip-yield model (Equation (3.44)).

The Shih analysis shows that there is a unique relationship between J and CTOD for a given material. Thus these two quantities are equally valid crack-tip-characterizing parameters for elastic-plastic materials. The fracture toughness of a material can be quantified either by a critical value of J or CTOD.

The above analysis contains an apparent inconsistency. Equation (3.48) is based on the HRR singularity, which does not account for large geometry changes at the crack tip. Figure 3.12 indicates that the stresses predicted by the HRR theory are inaccurate for $r < 2\delta$, but the Shih analysis uses the HRR solution to evaluate displacements well within the large strain region. Crack-tip finite element analyses [14], however, are in general agreement with Equation (3.48). Thus the displacement fields predicted from the HRR theory are reasonably accurate, despite the large plastic strains at the crack tip.

3.4 CRACK-GROWTH RESISTANCE CURVES

Many materials with high toughness do not fail catastrophically at a particular value of J or CTOD. Rather, these materials display a rising R curve, where J and CTOD increase with crack growth. In metals, a rising R curve is normally associated with the growth and coalescence of microvoids. See Chapter 5 for a discussion of microscopic fracture mechanisms in ductile metals.

Figure 3.19 schematically illustrates a typical J resistance curve for a ductile material. In the initial stages of deformation, the R curve is nearly vertical; there is a small amount of apparent crack growth due to blunting. As J increases, the material at the crack tip fails locally and the crack advances further. Because the R curve is rising, the initial crack growth is usually stable, but an instability can be encountered later, as discussed below.

One measure of fracture toughness J_{lc} is defined near the initiation of stable crack growth. The precise point at which crack growth begins is usually ill-defined. Consequently, the definition of J_{lc} is somewhat arbitrary, much like a 0.2% offset yield strength. The corresponding CTOD near the initiation of stable crack growth is denoted δ_i by U.S. and British testing standards. Chapter 7 describes experimental measurements of J_{lc} and δ_i in more detail.

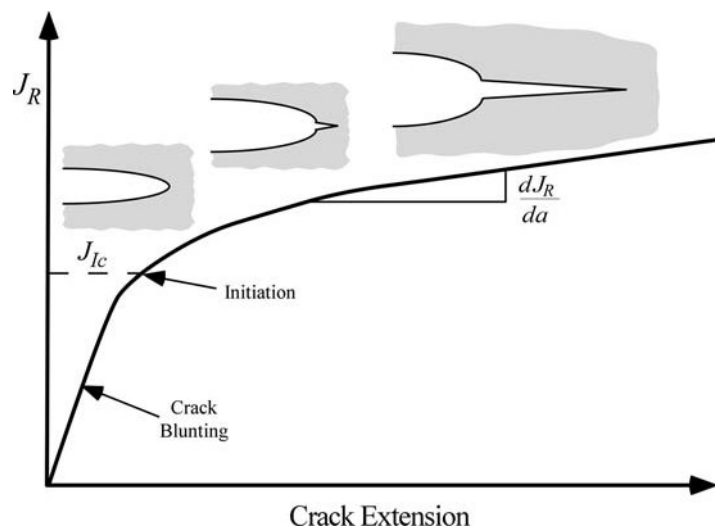


FIGURE 3.19 Schematic J resistance curve for a ductile material.

While initiation toughness provides some information about the fracture behavior of a ductile material, the entire R curve gives a more complete description. The slope of the R curve at a given amount of crack extension is indicative of the relative stability of the crack growth; a material with a steep R curve is less likely to experience unstable crack propagation. For J resistance curves, the slope is usually quantified by a dimensionless *tearing modulus*:

$$T_R = \frac{E}{\sigma_o^2} \frac{dJ_R}{da} \quad (3.49)$$

where the subscript R indicates a value of J on the resistance curve.

3.4.1 STABLE AND UNSTABLE CRACK GROWTH

The conditions that govern the stability of crack growth in elastic-plastic materials are virtually identical to the elastic case presented in Section 2.5. Instability occurs when the driving force curve is tangent to the R curve. As Figure 3.20 indicates, load control is usually less stable than displacement control. The conditions in most structures are somewhere between the extremes of load control and displacement control. The intermediate case can be represented by a spring in series with the structure, where remote displacement is fixed (Figure 2.12). Since the R curve slope has been represented by a dimensionless tearing modulus (Equation (3.49)), it is convenient to express the driving force in terms of an *applied tearing modulus*:

$$T_{app} = \frac{E}{\sigma_o^2} \left(\frac{dJ}{da} \right)_{\Delta_T} \quad (3.50)$$

where Δ_T is the total remote displacement defined as

$$\Delta_T = \Delta + C_m P \quad (3.51)$$

and C_m is the system compliance. The slope of the driving force curve for a fixed Δ_T is identical to the linear elastic case (Equation (2.35)), except that G is replaced by J :

$$\left(\frac{dJ}{da} \right)_{\Delta_T} = \left(\frac{\partial J}{\partial a} \right)_P - \left(\frac{\partial J}{\partial P} \right)_a \left(\frac{\partial \Delta}{\partial a} \right)_P \left[C_m + \left(\frac{\partial \Delta}{\partial P} \right)_a \right]^{-1} \quad (3.52)$$

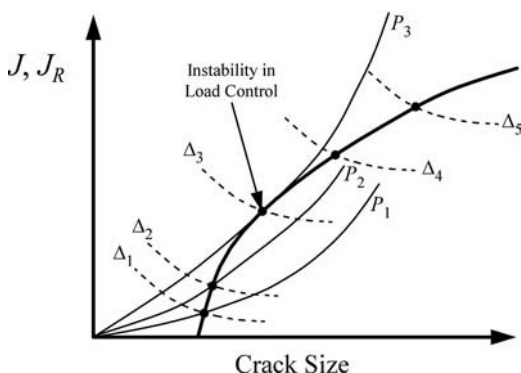


FIGURE 3.20 Schematic J driving force/ R curve diagram which compares load control and displacement control.

For load control, $C_m = \infty$, and the second term in Equation (3.52) vanishes:

$$\left(\frac{dJ}{da} \right)_{\Delta_T} = \left(\frac{\partial J}{\partial a} \right)_P$$

For displacement control, $C_m = 0$, and $\Delta_T = \Delta$. Equation (3.52) is derived in Appendix 2.2 for the linear elastic case.

The conditions during stable crack growth can be expressed as follows:

$$J = J_R \quad (3.53a)$$

and

$$T_{app} \leq T_R \quad (3.53b)$$

Unstable crack propagation occurs when

$$T_{app} > T_R \quad (3.54)$$

Chapter 9 gives practical guidance on assessing structural stability with Equation (3.50) to Equation (3.54). A simple example is presented below.

EXAMPLE 3.2

Derive an expression for the applied tearing modulus in the double cantilever beam (DCB) specimen with a spring in series (Figure 3.21), assuming linear elastic conditions.

Solution: From Example 2.1, we have the following relationships:

$$J = G = \frac{P^2 a^2}{BEI} \quad \text{and} \quad \Delta = G = \frac{2Pa^3}{3EI}$$

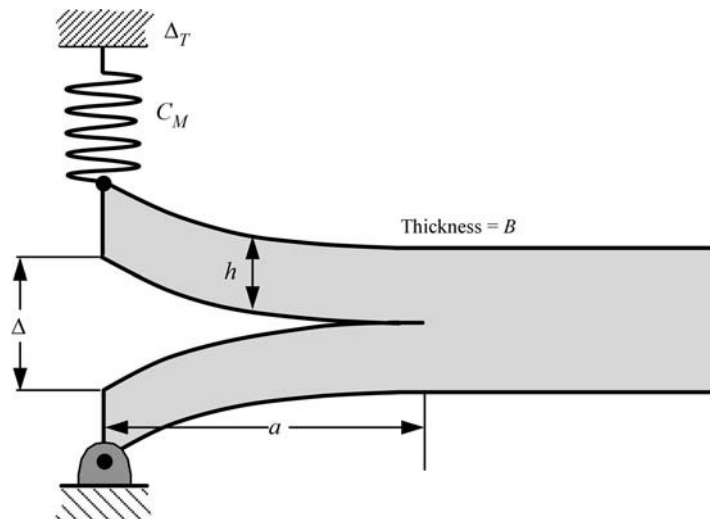


FIGURE 3.21 Double cantilever beam specimen with a spring in series.

Therefore, the relevant partial derivatives are given by

$$\left(\frac{\partial J}{\partial a}\right)_P = \frac{2P^2a}{BEI}$$

$$\left(\frac{\partial J}{\partial P}\right)_a = \frac{2Pa^2}{BEI}$$

$$\left(\frac{\partial \Delta}{\partial a}\right)_P = \frac{2Pa^2}{EI}$$

$$\left(\frac{\partial \Delta}{\partial P}\right)_a = \frac{2a^3}{3EI}$$

Substituting the above relationships into Equation (3.50) and Equation (3.52) gives

$$T_{app} = \frac{2P^2a}{\sigma_o^2 BI} \left\{ 1 - \frac{2a^3}{EI} \left[C_M + \frac{2a^3}{3EI} \right]^{-1} \right\}$$

As discussed in Section 2.5, the point of instability in a material with a rising R curve depends on the size and geometry of the cracked structure; a critical value of J at instability is not a material property if J increases with crack growth. It is usually assumed that the R curve, including the J_{lc} value, is a material property, independent of the configuration. This is a reasonable assumption, within certain limitations.

3.4.2 COMPUTING J FOR A GROWING CRACK

The geometry dependence of a J resistance curve is influenced by the way in which J is calculated. The equations derived in Section 3.2.5 are based on the pseudo energy release rate definition of J and are valid only for a stationary crack. There are various ways to compute J for a growing crack, including the deformation J and the far-field J , which are described below. The former method is typically used to obtain experimental J resistance curves.

Figure 3.22 illustrates the load-displacement behavior in a specimen with a growing crack. Recall that the J integral is based on a deformation plasticity (or nonlinear elastic) assumption for material behavior. Consider point A on the load-displacement curve in Figure 3.22. The crack has grown to a length a_1 from an initial length a_0 . The cross-hatched area represents the energy that would be released if the material were elastic. In an elastic-plastic material, only the elastic portion of this energy is released; the remainder is dissipated in a plastic wake that forms behind the growing crack (see Figure 2.6(b) and Figure 3.25).

In an elastic material, all quantities, including strain energy, are independent of the loading history. The energy absorbed during crack growth in an elastic-plastic material, however, exhibits a history dependence. The dashed curve in Figure 3.22 represents the load-displacement behavior when the crack size is fixed at a_1 . The area under this curve is the strain energy in an elastic material; this energy depends only on the current load and crack length:

$$U_D = U_D(P, a) = \left(\int_0^\Delta P d\Delta \right)_{a=a_1} \quad (3.55)$$

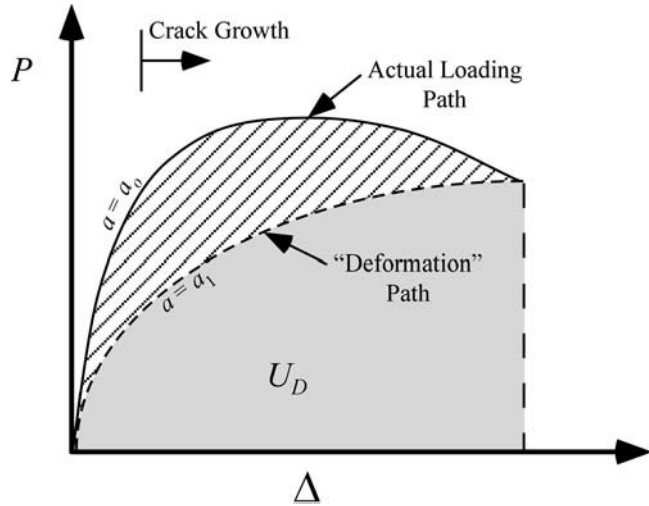


FIGURE 3.22 Schematic load-displacement curve for a specimen with a crack that grows to a_l from an initial length a_o . U_D represents the strain energy in a nonlinear elastic material.

where the subscript D refers to the deformation theory. Thus the J integral for a nonlinear elastic body with a growing crack is given by

$$\begin{aligned} J_D &= -\frac{1}{B} \left(\frac{\partial U_D}{\partial a} \right)_\Delta \\ &= \frac{\eta U_D}{Bb} \end{aligned} \quad (3.56a)$$

or

$$J_D = \frac{K_L^2}{E'} + \frac{\eta_p U_{D(p)}}{Bb} \quad (3.56b)$$

where b is the *current* ligament length. When the J integral for an elastic-plastic material is defined by Equation (3.56), the history dependence is removed and the energy release rate interpretation of J is restored. The *deformation J* is usually computed from Equation (3.56b) because no correction is required on the elastic term as long as K_L is determined from the current load and crack length. The calculation of $U_{D(p)}$ is usually performed incrementally, since the deformation theory load-displacement curve (Figure 3.22 and Equation (3.55)) depends on the crack size. Specific procedures for computing the deformation J are outlined in Chapter 7.

One can determine a far-field J from the contour integral definition of Equation (3.19), which may differ from J_D . For a deeply cracked bend specimen, Rice et al. [15] showed that the far-field J contour integral in a rigid, perfectly plastic material is given by

$$J_f = 0.73\sigma_o \int_0^\Omega b \, d\Omega \quad (3.57)$$

where the variation in b during the loading history is taken into account. The deformation theory leads to the following relationship for J in this specimen:

$$J_D = 0.73\sigma_o b \Omega \quad (3.58)$$

The two expressions are obviously identical when the crack is stationary.

Finite element calculations of Dodds et al. [16, 17] for a three-point bend specimen made from a strain hardening material indicate that J_f and J_D are approximately equal for moderate amounts of crack growth. The J integral obtained from a contour integration is path-dependent when a crack is growing in an elastic-plastic material, however, and tends to zero as the contour shrinks to the crack tip. See Appendix 4.2 for a theoretical explanation of the path dependence of J for a growing crack in an inelastic material.

There is no guarantee that either the deformation J_D or J_f will uniquely characterize crack-tip conditions for a growing crack. Without this single-parameter characterization, the J - R curve becomes geometry dependent. The issue of J validity and geometry dependence is explored in detail in Section 3.5 and Section 3.6.

3.5 J-CONTROLLED FRACTURE

The term *J-controlled fracture* corresponds to situations where J completely characterizes crack-tip conditions. In such cases, there is a unique relationship between J and CTOD (Section 3.3); thus J -controlled fracture implies CTOD-controlled fracture, and vice versa. Just as there are limits to LEFM, fracture mechanics analyses based on J and CTOD become suspect when there is excessive plasticity or significant crack growth. In such cases, fracture toughness and the J -CTOD relationship depend on the size and geometry of the structure or test specimen.

The required conditions for J -controlled fracture are discussed below. Fracture initiation from a stationary crack and stable crack growth are considered.

3.5.1 STATIONARY CRACKS

Figure 3.23 schematically illustrates the effect of plasticity on the crack tip stresses; $\log(\sigma_{yy})$ is plotted against the normalized distance from the crack tip. The characteristic length scale L corresponds to the size of the structure; for example, L could represent the uncracked ligament length. Figure 3.23(a) shows the small-scale yielding case, where both K and J characterize crack-tip conditions. At a short distance from the crack tip, relative to L , the stress is proportional to $1/\sqrt{r}$; this area is called the *K-dominated region*. Assuming monotonic, quasistatic loading, a J -dominated region occurs in the plastic zone, where the elastic singularity no longer applies. Well inside of the plastic zone, the HRR solution is approximately valid and the stresses vary as $r^{-1/(n+1)}$. The finite strain region occurs within approximately 2δ from the crack tip, where large deformation invalidates the HRR theory. In small-scale yielding, K uniquely characterizes crack-tip conditions, despite the fact that the $1/\sqrt{r}$ singularity does not exist all the way to the crack tip. Similarly, J uniquely characterizes crack-tip conditions even though the deformation plasticity and small strain assumptions are invalid within the finite strain region.

Figure 3.23(b) illustrates elastic-plastic conditions, where J is still approximately valid, but there is no longer a K field. As the plastic zone increases in size (relative to L), the K -dominated zone disappears, but the J -dominated zone persists in some geometries. Thus although K has no meaning in this case, the J integral is still an appropriate fracture criterion. Since J dominance implies CTOD dominance, the latter parameter can also be applied in the elastic-plastic regime.

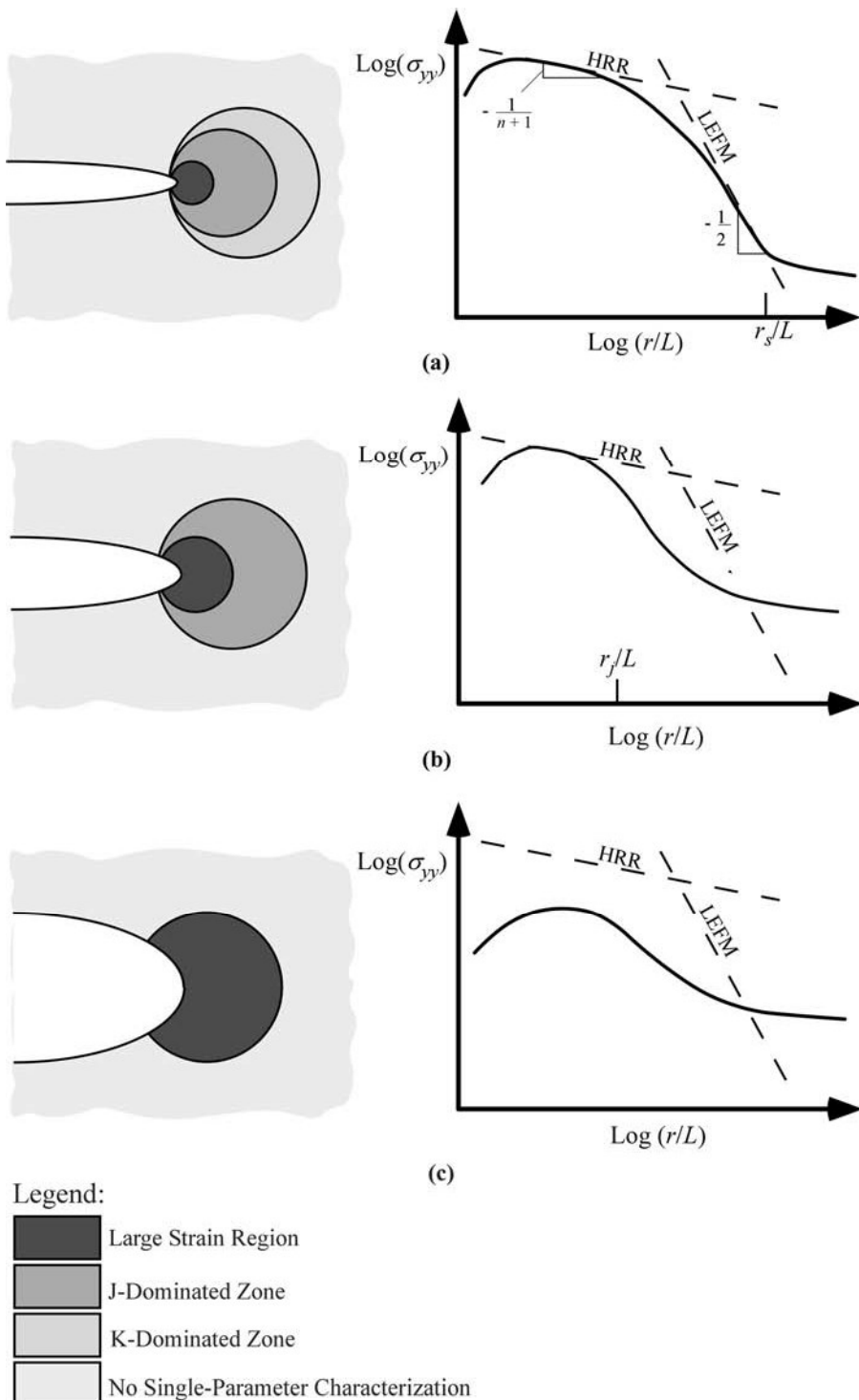


FIGURE 3.23 Effect of plasticity on the crack-tip stress fields: (a) small-scale yielding, (b) elastic-plastic conditions, and (c) large-scale yielding.

With large-scale yielding (Figure 3.23(c)), the size of the finite strain zone becomes significant relative to L , and there is no longer a region uniquely characterized by J . Single-parameter fracture mechanics is invalid in large-scale yielding, and critical J values exhibit a size and geometry dependence.

In certain configurations, the K and J zones are vanishingly small, and a single-parameter description is not possible except at very low loads. For example, a plate loaded in tension with a through-thickness crack is not amenable to a single-parameter description, either by K or J . Example 2.7 and Figure 2.39 indicate that the stress in the x direction in this geometry deviates significantly from the elastic singularity solution at small distances from the crack tip because of a compressive transverse (T) stress. Consequently the K -dominated zone is virtually nonexistent. The T stress influences stresses inside the plastic zone, so a highly negative T stress also invalidates a single-parameter description in terms of J . See Section 3.61 for further details about the T stress.

Recall Section 2.10.1, where a free-body diagram was constructed from a disk-shaped region removed from the crack tip of a structure loaded in small-scale yielding. Since the stresses on the boundary of this disk exhibit a $1/\sqrt{r}$ singularity, K_I uniquely defines the stresses and strains within the disk. For a given material,⁵ dimensional analysis leads to the following functional relationship for the stress distribution within this region:

$$\frac{\sigma_{ij}}{\sigma_o} = F_{ij}\left(\frac{K_I^2}{\sigma_o^2 r}, \theta\right) \quad \text{for } 0 \leq r \leq r_s(\theta) \quad (3.59)$$

where r_s is the radius of the elastic singularity dominated zone, which may depend on θ . Note that the $1/\sqrt{r}$ singularity is a special case of F , which exhibits a different dependence on r within the plastic zone. Invoking the relationship between J and K_I for small-scale yielding (Equation 3.18) gives

$$\frac{\sigma_{ij}}{\sigma_o} = F_{ij}\left(\frac{E' J}{\sigma_o^2 r}, \theta\right) \quad \text{for } 0 \leq r \leq r_J(\theta) \quad (3.60)$$

where r_J is the radius of the J -dominated zone. The HRR singularity (Equation (3.24a)) is a special case of Equation (3.60), but stress exhibits a $r^{-1/(n+1)}$ dependence only over a limited range of r .

For small-scale yielding, $r_s = r_J$, but r_s vanishes when the plastic zone engulfs the elastic singularity dominated zone. The J -dominated zone usually persists longer than the elastic singularity zone, as Figure 3.23 illustrates.

It is important to emphasize that the J dominance at the crack tip does not require the existence of an HRR singularity. In fact, J dominance requires only that Equation (3.60) is valid in the *process zone* near the crack tip, where the microscopic events that lead to fracture occur. The HRR singularity is merely one possible solution to the more general requirement that J uniquely define crack-tip stresses and strains. The flow properties of most materials do not conform to the idealization of a Ramberg-Osgood power law, upon which the HRR analysis is based. Even in a Ramberg-Osgood material, the HRR singularity is valid over a limited range; large strain effects invalidate the HRR singularity close to the crack tip, and the computed stress lies below the HRR solution at greater distances. The latter effect can be understood by considering the analytical technique employed by Hutchinson [7], who represented the stress solution as an infinite series and showed that the leading term in the series was proportional to $r^{-1/(n+1)}$ (see Appendix 3.4). This singular term dominates as $r \rightarrow 0$; higher-order terms are significant for moderate values of r . When the computed stress field deviates from HRR, it still scales with $J/(\sigma_o r)$, as required by Equation (3.60). Thus J dominance does not necessarily imply agreement with the HRR fields.

⁵ A complete statement of the functional relationship of σ_{ij} should include all material flow properties (e.g., α and n for a Ramberg-Osgood material). These quantities were omitted from Equation (3.59) and Equation (3.60) for the sake of clarity, since material properties are assumed to be fixed in this problem.

Equation (3.59) and Equation (3.60) gradually become invalid as specimen boundaries interact with the crack tip. We can apply dimensional arguments to infer when a single-parameter description of crack-tip conditions is suspect. As discussed in Chapter 2, the LEFM solution breaks down when the plastic-zone size is a significant fraction of in-plane dimensions. Moreover, the crack-tip conditions evolve from plane strain to plane stress as the plastic-zone size grows to a significant fraction of the thickness. The J integral becomes invalid as a crack-tip-characterizing parameter when the large strain region reaches a finite size relative to in-plane dimensions. Section 3.6 provides quantitative information on size effects.

3.5.2 J -CONTROLLED CRACK GROWTH

According to the dimensional argument in the previous section, J -controlled conditions exist at the tip of a stationary crack (loaded monotonically and quasistatically), provided the large strain region is small compared to the in-plane dimensions of the cracked body. Stable crack growth, however, introduces another length dimension, i.e., the change in the crack length from its original value. Thus J may not characterize crack-tip conditions when the crack growth is significant compared to the in-plane dimensions. Prior crack growth should not have any adverse effects in a purely elastic material, because the local crack-tip fields depend only on current conditions. However, prior history does influence the stresses and strains in an elastic-plastic material. Therefore, we might expect the J integral theory to break down when there is a combination of significant plasticity and crack growth. This heuristic argument based on dimensional analysis agrees with experiment and with more complex analyses.

Figure 3.24 illustrates crack growth under J -controlled conditions. The material behind the growing crack tip has unloaded elastically. Recall Figure 3.7, which compares the unloading behavior of nonlinear elastic and elastic-plastic materials; the material in the unloading region of Figure 3.24 obviously violates the assumptions of deformation plasticity. The material directly in front of the crack also violates the single-parameter assumption because the loading is highly nonproportional, i.e., the various stress components increase at different rates and some components actually decrease. In order for the crack growth to be J controlled, the elastic unloading and nonproportional plastic loading regions must be embedded within a zone of J dominance. When the crack grows out of the zone of J dominance, the measured R curve is no longer uniquely characterized by J .

In small-scale yielding, there is always a zone of J dominance because the crack-tip conditions are defined by the elastic stress intensity, which depends only on the current values of the load and crack size. The crack never grows out of the J -dominated zone as long as all the specimen boundaries are remote from the crack tip and the plastic zone.

Figure 3.25 illustrates three distinct stages of crack growth resistance behavior in small-scale yielding. During the initial stage the crack is essentially stationary; the finite slope of the R curve

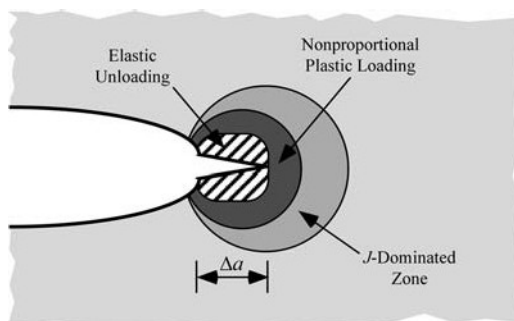


FIGURE 3.24 J -controlled crack growth.

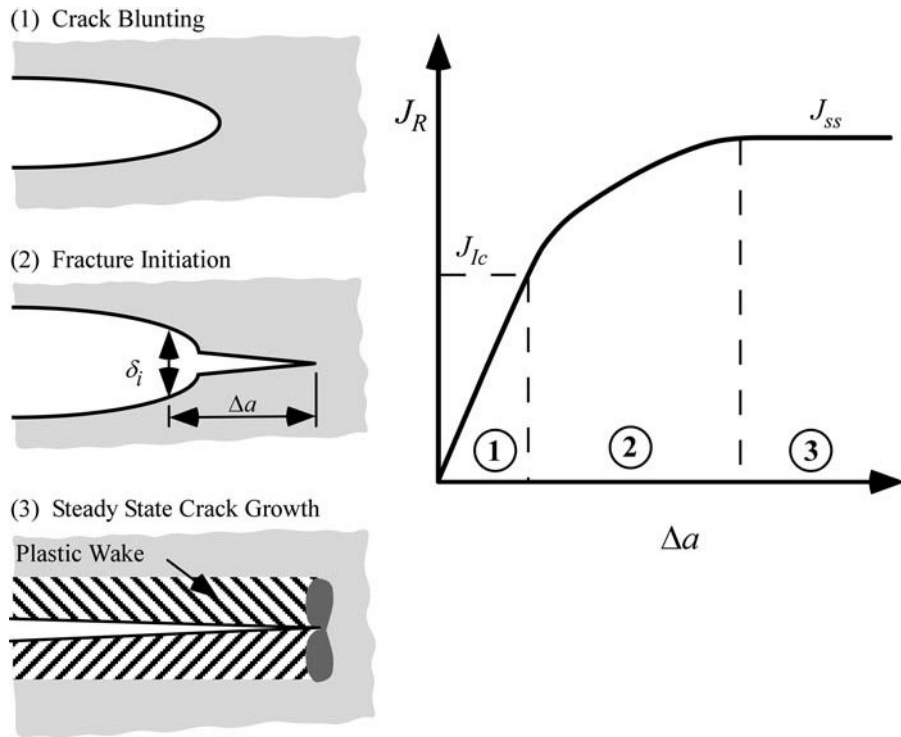


FIGURE 3.25 Three stages of crack growth in an infinite body.

is caused by blunting. The crack-tip fields for Stage 1 are given by

$$\frac{\sigma_{ij}}{\sigma_o} = F_{ij}^{(1)}\left(\frac{E'J}{\sigma_o^2 r}, \theta\right) \quad (3.61)$$

which is a restatement of Equation (3.60). The crack begins to grow in Stage 2. The crack-tip stresses and strains are probably influenced by the original blunt crack tip during the early stages of crack growth. Dimensional analysis implies the following relationship:

$$\frac{\sigma_{ij}}{\sigma_o} = F_{ij}^{(2)}\left(\frac{E'J}{\sigma_o^2 r}, \theta, \frac{\Delta a}{\delta_i}\right) \quad (3.62)$$

where δ_i is the CTOD at initiation of stable tearing. When the crack grows well beyond the initial blunted tip, a steady-state condition is reached, where the local stresses and strains are independent of the extent of crack growth:

$$\frac{\sigma_{ij}}{\sigma_o} = F_{ij}^{(3)}\left(\frac{E'J}{\sigma_o^2 r}, \theta\right) \quad (3.63)$$

Although Equation (3.61) and Equation (3.63) would predict identical conditions in the elastic-singularity zone, the material in the plastic zone at the tip of a growing crack is likely to experience a different loading history from the material in the plastic zone of a blunting stationary crack; thus $F^{(1)} \neq F^{(3)}$ as $r \rightarrow 0$. During steady-state crack growth, a plastic zone of constant size sweeps through

the material, leaving a plastic wake, as illustrated in Figure 3.25. The R curve is flat; J does not increase with crack extension, provided the material properties do not vary with position. Appendix 3.5.2 presents a formal mathematical argument for a flat R curve during steady-state growth; a heuristic explanation is given below.

If Equation (3.63) applies, J uniquely describes crack-tip conditions, independent of crack extension. If the material fails at some critical combination of stresses and strains, it follows that local failure at the crack tip must occur at a critical J value, as in the stationary crack case. This critical J value must remain constant with crack growth. A rising or falling R curve would imply that the local material properties varied with position.

The second stage in Figure 3.25 corresponds to the transition between the blunting of a stationary crack and crack growth under steady state conditions. A rising R curve is possible in Stage 2. For small-scale yielding conditions the R curve depends only on crack extension:

$$J_R = J_R(\Delta a) \quad (3.64)$$

That is, the J - R curve is a material property.

The steady-state limit is usually not observed in laboratory tests on ductile materials. In typical test specimens, the ligament is fully plastic during crack growth, thereby violating the small-scale yielding assumption. Moreover, the crack approaches a finite boundary while still in Stage 2 growth. Enormous specimens would be required to observe steady-state crack growth in tough materials.

3.6 CRACK-TIP CONSTRAINT UNDER LARGE-SCALE YIELDING

Under small-scale yielding conditions, a single parameter (e.g., K , J , or CTOD) characterizes crack-tip conditions and can be used as a geometry-independent fracture criterion. Single-parameter fracture mechanics breaks down in the presence of excessive plasticity, and the fracture toughness depends on the size and geometry of the test specimen.

McClintock [18] applied the slip line theory to estimate the stresses in a variety of configurations under plane strain, fully plastic conditions. Figure 3.26 summarizes some of these results. For small-scale yielding (Figure 3.26(a)), the maximum stress at the crack tip is approximately $3\sigma_o$ in a nonhardening material. According to the slip line analysis, a deeply notched double-edged notched tension (DENT) panel, illustrated in Figure 3.26(b), maintains a high level of triaxiality under fully plastic conditions, such that the crack-tip conditions are similar to the small-scale yielding case. An edge-cracked plate in bending (Figure 3.26(c)) exhibits slightly less stress elevation, with the maximum principal stress approximately $2.5\sigma_o$. A center-cracked panel in pure tension (Figure 3.26(d)) is incapable of maintaining significant triaxiality under fully plastic conditions.

The results in Figure 3.26 indicate that for a nonhardening material under fully yielded conditions, the stresses near the crack tip are not unique, but depend on geometry. Traditional fracture mechanics approaches recognize that the stress and strain fields remote from the crack tip may depend on geometry, but it is assumed that the near-tip fields have a similar form in all configurations that can be scaled by a single parameter. The single-parameter assumption is obviously not valid for nonhardening materials under fully plastic conditions, because the near-tip fields depend on the configuration. Fracture toughness, whether quantified by J , K , or CTOD, must also depend on the configuration.

The prospects for applying fracture mechanics in the presence of large-scale yielding are not quite as bleak as the McClintock analysis indicates. The configurational effects on the near-tip fields are much less severe when the material exhibits strain hardening. Moreover, single-parameter fracture mechanics may be approximately valid in the presence of significant plasticity, provided the specimen maintains a relatively high level of triaxiality. Both the DENT specimen and the edge-cracked plate in bending (SE(B)) apparently satisfy this requirement. Most laboratory measurements